D-GAP: Improving Out-of-Domain Robustness via Dataset-Agnostic and Gradient-Guided Augmentation in Amplitude and Pixel Spaces

Ruoqi Wang HKUST(GZ)

rwang280@connect.hkust-gz.edu.cn

Shaojie Guo ECNU

52275904013@stu.ecnu.edu.cn

Haitao Wang SYSU

wanght39@mail2.sysu.edu.cn

Qiong Luo HKUST(GZ) & HKUST

luo@cse.ust.hk

Abstract

Out-of-domain (OOD) robustness is challenging to achieve in real-world computer vision applications, where shifts in image background, style, and acquisition instruments always degrade model performance. Generic augmentations show inconsistent gains under such shifts, whereas dataset-specific augmentations require expert knowledge and prior analysis. Moreover, prior studies show that neural networks adapt poorly to domain shifts because they exhibit a learning bias to domain-specific frequency components. Perturbing frequency values can mitigate such bias but overlooks pixel-level details, leading to suboptimal performance. To address these problems, we propose **D-GAP** (**D**ataset-agnostic and **G**radient-guided augmentation in Amplitude and Pixel spaces), improving OOD robustness by introducing targeted augmentation in both the amplitude space (frequency space) and pixel space. Unlike conventional handcrafted augmentations, D-GAP computes sensitivity maps in the frequency space from task gradients, which reflect how strongly the model responds to different frequency components, and uses the maps to adaptively interpolate amplitudes between source and target samples. This way, D-GAP reduces the learning bias in frequency space, while a complementary pixel-space blending procedure restores fine spatial details. Extensive experiments on four real-world datasets and three domainadaptation benchmarks show that D-GAP consistently outperforms both generic and dataset-specific augmentations, improving average OOD performance by +5.3% on realworld datasets and +1.8% on benchmark datasets.

1. Introduction

In real-world applications, the distributions in the training datasets often differ from those in other deployment environments because of the shifts in background and acquisition instruments [15, 21]. In such out-of-distribution (OOD) settings, models trained on source domains always degrade when applied to unlabeled target domains. For example, in wildlife monitoring, ecologists use models to classify species of camera trap images, but these models often show significant accuracy drops when applied to new locations [2]. Annotated data are usually available only for a limited subset of cameras, which may not contain the diversity of environments in the unlabeled target domains. In this paper, we focus on improving OOD robustness in domain adaptation, where we have labeled data from source domains and unlabeled data from target domains.

Data augmentation is a common strategy for improving OOD robustness of models, but designing effective augmentations remains challenging. Generic augmentations of images (e.g., RandAugment [4], CutMix [38], FACT [35], SAM [33]) improves the performance across datasets to various degrees [8, 11, 32], whereas domain-invariance methods [8, 13, 36, 37, 40] yield limited improvements, especially on real-world domain shifts [7]. Although some dataset-specific augmentation methods [7, 21] can improve OOD performance, they often need expert knowledge and prior analysis of the dataset, which makes these methods hard to scale or apply to new datasets. These limitations highlight the need for more general, dataset-agnostic methods to improve OOD robustness across diverse real-world settings.

Prior studies show that neural networks tend to learn biasedly from different frequency components depending on the dataset's frequency characteristics [10, 20, 31]. Such spectral bias causes the model to overfit domain-specific

frequency components in the frequency spectrum, leading to poor generalization when the target domain has different frequency distributions. As such, we consider that this bias can be reduced by perturbing the data distribution in the frequency space. However, frequency variations only reflect texture and style changes, overlooking spatial details. Since the pixel space preserves spatial details and localized pixellevel features which are complementary to frequency information, combining both spaces may address global and local domain shifts simultaneously. Building on this intuition, we propose D-GAP (Dataset-agnostic and Gradient-guided Augmentation in Amplitude and Pixel spaces), a domain adaptation framework that improves OOD robustness by introducing targeted augmentations in both the frequency and the pixel spaces. Unlike previous targeted augmentations that depend on manually designed, dataset-specific rules, and work solely in frequency or pixel space, D-GAP automatically adapts to domain shifts from data itself, without the need for expert knowledge or prior analysis.

Specifically, given two images from different domains, in the frequency space, we introduce a gradient-adaptive mechanism in the frequency space that computes frequency sensitivity maps from the task gradients with respect to the amplitude. These sensitivity maps represent how strongly the model responds to different frequency components. Instead of interpolating two spectra with a fixed or random ratio, D-GAP adjusts the interpolation strength at each frequency according to its sensitivity value: more sensitive frequency components are more strongly mixed with targetdomain amplitudes, while less sensitive ones are more preserved. This mechanism enables the model to suppress domain-specific spectral learning bias by perturbing biased with varying intensities. This gradient-guided interpolation creates frequency-space augmentations that adaptively keep the main content of the source image while adding features from target domains. However, frequency blending and reconstruction sometimes introduce artifacts and blurring. As such, we apply pixel-space blending to add complementary spatial pixel-level information. The final augmented image is then obtained by blending these two results from the frequency space and the pixel space.

We evaluate our method on four real-world datasets: wildlife recognition (iWildCam [3, 22]), tumor detection (Camelyon17 [1, 22]), bird species recognition (BirdCalls [7, 14]), and galaxy morphology classification (Galaxy10 DECaLS & SDSS [12]). Extensive experiments demonstrate that D-GAP consistently outperforms other baselines. Compared to other generic methods, D-GAP achieves improvements in OOD performance, including +2.1% gains on iWildCam, +4.2% on Camelyon17, +5.6% on BirdCalls, and +9.3% on Galaxy10. Also, it surpasses dataset-specific augmentation strategies tailored for different datasets. Additionally, D-GAP also makes average gains of +1.8% ac-

curacy on standard benchmark datasets (PACS [17], Office-Home [29], and Digits-DG [40]), showing its improvement across diverse distribution shifts. We further analyse the effectiveness of D-GAP connecting same-class cross-domain samples while separating different-class examples.

Our work makes the following contributions: (1) We propose D-GAP, a dataset-agnostic target augmentation method that works in both the frequency and pixel spaces, through gradient-guided amplitude interpolation and spatial blending, respectively. (2) Our method is general and adaptive, with strong performance in real-world applications without dataset-specific manipulation. (3) We achieve state-of-the-art results on both real-world and general benchmark datasets, significantly outperforming other baselines.

2. Background and Formulation

2.1. Feature Decomposition

To better understand how models perform under domain shifts, we use the feature decomposition framework [7], which categorizes input features based on their dependence on the label and domain. Specifically, input features can be decomposed into four types based on their dependence on the label and the domain: (1) features that are label-dependent and domain-independent (x_{obj}) ; (2) label-dependent and domain-dependent features $(x_{\text{d:robust}})$; (3) label-independent and domain-dependent features $(x_{\text{d:spu}})$; and (4) label-independent and domain-independent features (x_{noise}) . We formalize these relationships via their (in)dependence with the label y and domain d:

$$x_{ ext{obj}}, \ x_{ ext{d:robust}} \not\perp y, \quad x_{ ext{noise}}, \ x_{ ext{d:spu}} \perp y,$$
 $x_{ ext{d:robust}}, \ x_{ ext{d:spu}} \not\perp d, \quad x_{ ext{obj}}, \ x_{ ext{noise}} \perp d.$

Models should focus on both $x_{\rm obj}$ and $x_{\rm d:robust}$ while avoiding reliance on spurious or noisy features [7]. We later analyse these relationships using a connectivity-based framework (Section 2.4 and 5.1) to evaluate how augmentations influence these label/domain dependent features.

2.2. Datasets

Real-World Datasets. As shown in Figure 1, we test our method on four real-world datasets in this paper: iWild-Cam [3, 15] – wildlife species classification with location-related background shifts. Camelyon17 [1, 15] – tumor identification across hospitals with stain and density variations. BirdCalls [7, 14] – bird species recognition under habitat and microphone domain noise. Galaxy10 [12] – galaxy morphology classification across telescopes differing in resolution and color profile. Each dataset presents distinct domain shifts such as environmental background, staining style, recording device, or instrument differences. More dataset details are provided in Appendix Section B.

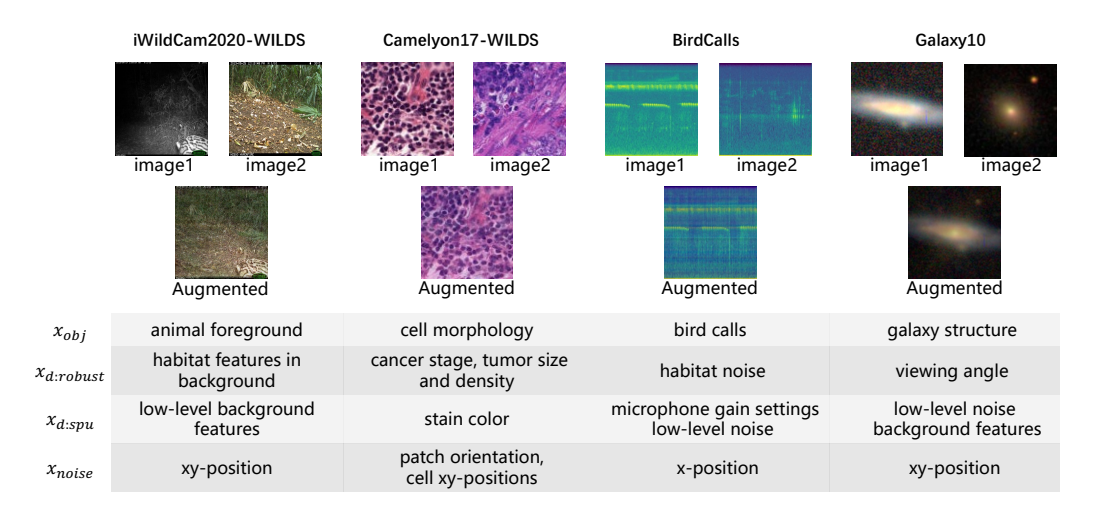


Figure 1. Feature decomposition and augmentation examples. *Top:* For each dataset (iWildCam, Camelyon17, BirdCalls, Galaxy10), we show a source image, its corresponding augmented image generated by our method. *Bottom:* Based on the decomposition framework [25], we annotate representative features in the datasets across x_{obj} , $x_{d:\text{robust}}$, $x_{d:\text{spu}}$, x_{noise} . Our method effectively randomizes $x_{d:\text{spu}}$, varies $x_{d:\text{robust}}$ while preserving or x_{obj} .

Additional Benchmark Datasets. In addition to the four real-world datasets used throughout this paper, we further evaluate our method on three standard benchmarks: PACS [17], Office-Home [29], and Digits-DG [40]. Compared to our four real-world datasets that cover diverse real-world scenario and deployment-related shifts, these benchmarks datasets focus on visual recognition with well-studied style variations. More dataset details are provided in Appendix Section B.

2.3. Targeted Augmentations

Some dataset-specific augmentation methods [7, 21] can improve OOD performance on real-world applications. However, they often need expert knowledge and prior analysis of the dataset, which makes these methods hard to scale or apply to new datasets. For instance, in wildlife recognition, some methods randomize the background of camera trap images to mitigate spurious correlations between results and location-specific terrains or lighting conditions. Such a target augmentation helps the model to focus on the animal foreground. However, it depends on the segmentation of foreground and background, restricting its application to datasets without foreground annotations. Similarly, in tumor identification from histopathology slides, Stain Color Jitter can deal with stain color variations across hospitals [28]. It perturbs images within the hematoxylin and eosin staining features to overcome color-related domain biases, while preserving morphological features [7]. However, it requires expert knowledge of staining chemistry and color editing. These examples show that while dataset-specific augmentations can be effective, they are difficult to generalize.

2.4. Connectivity

To better understand how data augmentations impact cross-domain generalization, we adopt the concept of *connectivity* [25]. We define connectivity between a class-domain pair $((y_1, d_1), (y_2, d_2))$ under four conditions:

$$\begin{cases} \rho: y_1=y_2, \ d_1=d_2. & \text{(same class, same domain)} \\ \alpha: y_1=y_2, \ d_1\neq d_2. & \text{(same class, different domains)} \\ \beta: y_1\neq y_2, \ d_1=d_2. & \text{(different classes, same domain)} \\ \gamma: y_1\neq y_2, \ d_1\neq d_2. & \text{(different classes, different domains)} \end{cases}$$

Here, each of the ρ , α , β , γ values indicates how "connected" a pair is. Shen et al. [25] show that the ratios $\frac{\alpha}{\gamma}$ and $\frac{\beta}{\gamma}$ exhibit strong empirical correlation with OOD accuracy. In this work, we follow this approach to show how our augmentation changes the connectivity of the data. More details on the computation of connectivity are presented in Section 5.1 and the Appendix Section D. To improve OOD robustness, the model must randomize features that depend on specific domains while preserving taskrelevant information. Specifically, in feature decomposition [25], we randomize domain-dependent features $(x_{d:spu})$ and keep label-relevant ones $(x_{obj}, x_{d:robust})$. As shown in Figure 2, we observe that amplitude mixing in frequency domain (Details of the mixing strategy are provided in Section 3.) preserves task-relevant semantic structure [35] (x_{obj} and $x_{d:robust}$), while effectively randomizing $x_{d:spu}$. However, solely frequency mixing may introduce artifacts and blurring (as examples in Figure 2 and 3), influencing the extraction of detailed features.

To address the problem, we add pixel-space mixing as

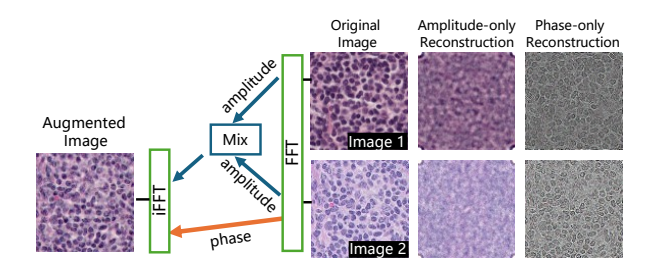


Figure 2. The figure shows the amplitude-only and phase-only reconstructions of the two input images, and the process where the amplitudes of Image 1 and Image 2 are first mixed, and the mixed amplitude is combined with the phase of Image 2 to generate an augmentation of Image 2.

Table 1. Comparison of connectivity values and ratio on iWildCam dataset.

Datasets	$ \alpha$	β	γ	α/γ	β/γ
Original	0.007	0.008	0.021	0.33	0.38
Augmented	0.212	0.030	0.051	4.16	0.59

a complement, which brings back more pixel-level details and perturbs $x_{d:spu}$. However, it may influence x_{obj} and $x_{d:\text{robust}}$ as well. Therefore, we then define a tunable ratio (details are in Section 3). By combining the augmentation in both frequency and pixel spaces, our goal is to balance the label-relevant and domain-relevant shifts, achieving domain diversity while maintaining semantic identity. This dual-space augmentation enables fine-grained control over domain perturbation intensity and promotes robust feature learning across source and unseen domains. We then empirically evaluate our method by comparing the connectivity ratios $\frac{\alpha}{\gamma}$ and $\frac{\beta}{\gamma}$ of the augmented and unaugmented datasets. Results in Table 1 show that augmentation in frequency-pixel spaces can enhance the cross-domain connectivity, achieving domain diversity while maintaining label-relevant identity.

3. Method

In this section, we introduce the technical details of D-GAP, including Fourier transform preliminaries and details of each module in D-GAP, including the Gradient-guided Amplitude Mix, Pixel-Space Mixing, and the training framework.

3.1. **D-GAP**

Fourier Transform of Images. For an image x, its Fourier transformation $\mathcal{F}(x)$ is formulated as:

$$\mathcal{F}(x)(u,v) = \sum_{h=0}^{H-1} \sum_{w=0}^{W-1} x(h,w) e^{-j2\pi \left(\frac{hu}{H} + \frac{wv}{W}\right)}, \quad (2)$$

where (u,v) are coordinates in the frequency space. $\mathcal{F}^{-1}(x)$ denotes the corresponding inverse Fourier transformation. Both forward and inverse Fourier transforms can be efficiently computed via the Fast Fourier Transform (FFT) algorithm.

The amplitude and phase components of $\mathcal{F}(x)$ are computed respectively as:

$$\mathcal{A}(x)(u,v) = \left[R^2(x)(u,v) + I^2(x)(u,v)\right]^{1/2},$$

$$\mathcal{P}(x)(u,v) = \arctan\left(\frac{I(x)(u,v)}{R(x)(u,v)}\right).$$
(3)

where R(x) and I(x) denote the real and imaginary parts of $\mathcal{F}(x)$, respectively. For RGB images, the Fourier transform is applied to each channel separately.

Gradient-guided Amplitude Mix. Conventional frequency-based augmentations [33, 35] typically mix amplitudes of two images with a random intensity factor. While such random interpolation introduces diversity, it fails to distinguish how sensitive that the model is to each frequency component. Moreover, the interpolation ratio need to be manually constrained within a predefined range to avoid excessive distortion. To overcome these limitations, D-GAP performs a gradient-guided amplitude mix, adaptively adjusting the interpolation strength based on the model's sensitivity in the frequency space. The process of Gradient-guided Amplitude Mix is shown in Figure 3.

Given two source images x_1 and x_2 , we aim to augment x_1 by injecting the amplitude information of x_2 into a square region Ω_r in the Fourier space. Let f denote the classifier and $\mathcal{L}_{\text{task}}$ the supervised loss. We compute the gradient of the loss with respect to the source amplitude:

$$G(u,v) = \left| \frac{\partial \mathcal{L}_{task}(f(x_1), y)}{\partial A(x_1)(u, v)} \right|, \quad (u, v) \in \Omega_r.$$
 (4)

Here, G(u,v) measures the model's sensitivity to each frequency, which means how much the task loss would change if the amplitude at a specific frequency (u,v) were perturbed. In this paper, we call G(u,v) as **sensitivity map**. Large gradient values indicate that the model's prediction heavily depends on that frequency component, implying stronger spectral bias. This allows D-GAP to continuously regulate how much information to mix at each frequency.

Then after normalizing G and applying a sigmoid function

$$\tilde{G} = \frac{G - \mu(G)}{\sigma(G) + \varepsilon}, \quad D = \text{clip}(\text{Sigmoid}(\tilde{G}), d_{\min}, d_{\max}),$$
(5)

we obtain a gradient-based **mixing map** D(u, v) from the sensitivity map G(u, v) that adaptively controls the amplitude interpolation. In our design, higher sensitivity (larger

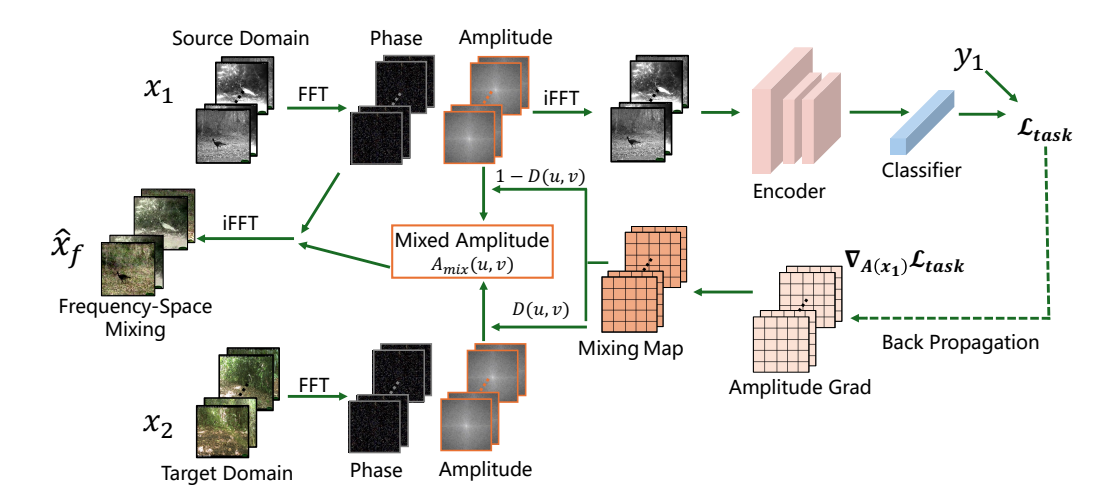


Figure 3. Overview of the Gradient-guided Amplitude Mix procedure. Given a source image x_1 and a target-domain image x_2 , we compute the Sensitivity Map G(u, v) and the Mixing Map D(u, v). The mixed amplitude is then combined with the phase of x_1 .

G(u,v)) leads to stronger interpolation from the target domain, encouraging the model to replace its frequency-biased components with cross-domain information. Conversely, D-GAP uses weaker interpolation in lower sensitivity regions to preserve non-biased features. The final adaptive interpolation is computed as:

$$A_{\text{mix}}(u, v) = (1 - D(u, v)) A(x_1)(u, v) + D(u, v) A(x_2)(u, v), \qquad (u, v) \in \Omega_r.$$
(6)

Finally, the mixed image is reconstructed as

$$\mathcal{F}_{\text{mix}}(u, v) = A_{\text{mix}}(u, v) e^{-jP(x_1)(u, v)},$$

$$\hat{x}_f = \mathcal{F}^{-1}(\mathcal{F}_{\text{mix}}).$$
(7)

Through this gradient-guided strategy, D-GAP adaptively perturbs spectral values with target domain more strongly where the model exhibits higher frequency bias. This data-driven, continuous modulation mitigates models' reliance on domain-specific spectral shortcuts, encouraging the model to learn more balanced and generalizable representations across domains.

Pixel-Space Mixing: Frequency blending sometimes introduces artifacts and blurring in the resulting augmentations. As a result, in addition to frequency-domain augmentation, we introduce a pixel-space mixing strategy to add more pixel-level details in the augmentation. Specifically, given a source image x and a target image x', we apply pixel-wise blending with ratio λ_1 :

$$\hat{x}_p = (1 - \lambda_1)x_1 + \lambda_1 x_2, \tag{8}$$

Then, we combine both pixel-space and frequency-space augmented images via a second-stage blending:

$$\hat{x} = (1 - \lambda_2)\hat{x}_f + \lambda_2\hat{x}_p,\tag{9}$$

This two-stage fusion allows us to perturb frequency bias while maintaining the semantic content of the original sample and the pixel details.

3.2. Training Framework

Our training strategy follows established practices in prior works [16, 21, 33, 35].

Real-world datasets. For real-world datasets (e.g., *iWildCam*, *Camelyon17*, *BirdCalls*, and *Galaxy10*), we use the **Linear Probing then Fine-Tuning (LP-FT)** strategy [16, 21]. We first train a linear classifier on frozen pretrained features to stabilize early optimization, then finetune both the encoder and classifier using D-GAP augmentations. This procedure improves OOD robustness by gradually adapting high-level representations to domain-diverse augmentations while preventing early-stage overfitting.

Common DG Benchmarks. For domain generalization benchmarks (i.e., *PACS*, *Office-Home*, *Digits-DG*), we follow previous works [33, 35] to train directly on the pretrained encoder without the LP-FT stage for fair comparisons. On these datasets, the pretrained model already provides a stable initialization, and applying D-GAP augmentations directly during training yields efficient adaptation and robust convergence.

4. Experiments

In this section, we first conduct comparisons between D-GAP and other recent methods on various datasets. We also conduct an ablation study to evaluate the contribution of each module in D-GAP. Finally, we conduct a connectivity analysis on empirical evidence of how our dual-space augmentation enhances cross-domain feature alignment.

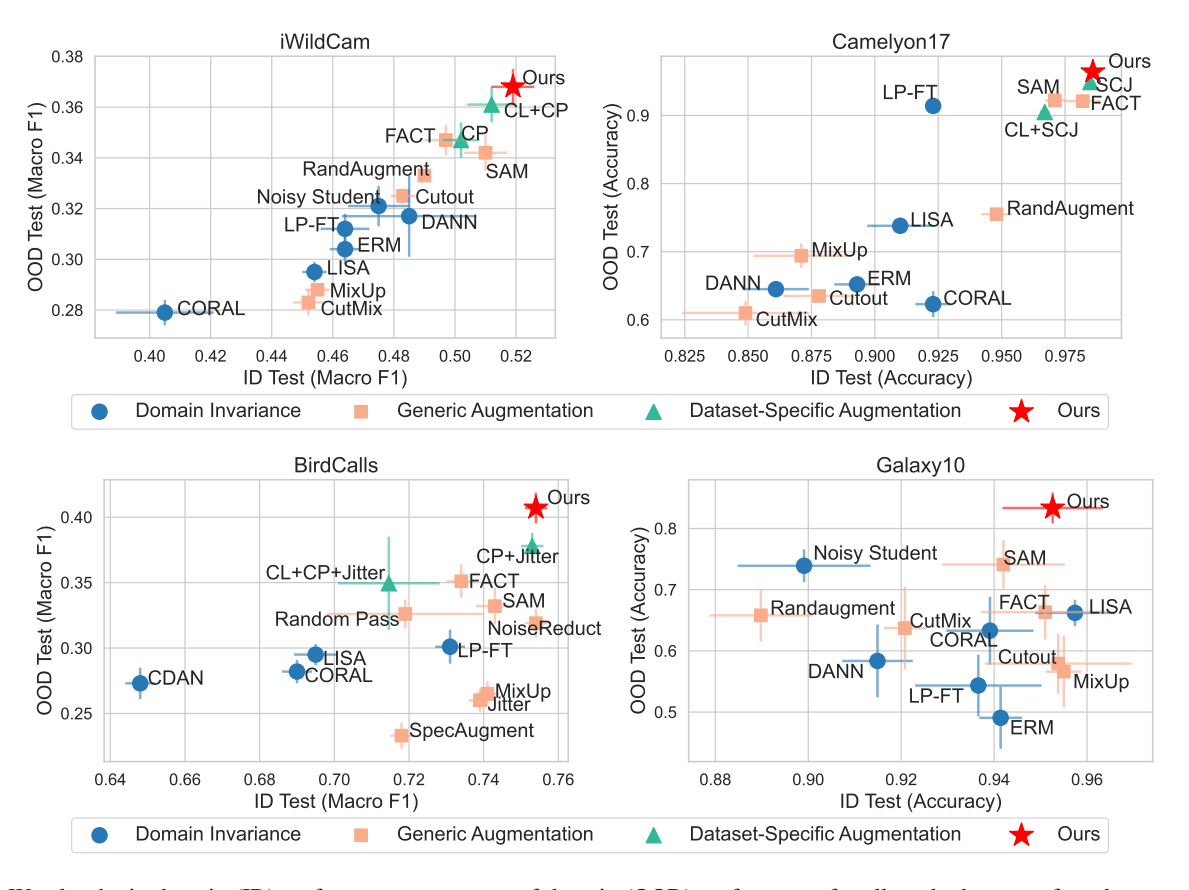


Figure 4. We plot the in-domain (ID) performance versus out-of-domain (OOD) performance for all methods across four datasets. Our method consistently outperforms all baselines in OOD generalization. 'CL' refers to 'Connect Later'. 'CP' refers to 'Copy Paste'. 'SCJ' refers to 'Stain Color Jitter'.

4.1. Experimental Settings

Platform: We conduct the experiments on a server with 128 AMD EPYC 7543 32-Core Processors, 512GB main memory, and eight NVIDIA RTX A6000 GPUs, each with 48GB device memory. The operating system is Ubuntu 22.04. Our model is implemented in PyTorch 2.1.0.

Evaluation Metrics: Following previous work [7, 21, 24, 30, 33, 35], we select metrics that best suit the characteristics of each dataset to ensure a comprehensive evaluation of model performance. We use F1 score and accuracy as evaluation metrics, depending on the nature of the task and dataset. The F1 score is used for iWildCam, BirdCalls datasets to account for class imbalance, and we use accuracy for Camelyon17, Galaxy10, PACS, Digits-DG and OfficeHome datasets.

Method under Comparison: We compare our method against various baseline approaches for domain generalization and out-of-domain (OOD) performance enhancement. These baselines include:

(1) **Generic Augmentations.** For real-world dataset iWildCam, Camelyon17 and Galaxy10, we compare our

approach with several commonly used augmentation techniques: RandAugment [4], CutMix [38], MixUp [39], Cutout [5], FACT [35], and SAM [33]. In the case of the BirdCalls dataset, we compare with MixUp, SpecAugment [19], random low/high pass filters, noise reduction [23], Jitter [7, 28], FACT [35], and SAM [33]. For the DG benchmark datasets, we compared with two state-of-the-art baselines FACT [35], and SAM [33].

- (2) **Dataset-Specific Targeted Augmentations.** We also compare our method with dataset-specific targeted augmentations [7] for real-world datasets: Copy-Paste for iWild-Cam, Stain Color Jitter for Camelyon17, and Copy-Paste + Jitter for BirdCalls. We also compare to the latest SOTA method Connect Later, which includes the dataset-specific targeted augmentations in the finetuning procedure after pretraining [21].
- (3) **Domain Invariance Baselines.** We compare to LISA [37], a method designed to encourage domain invariance by applying mixing augmentations to inputs of the same class across different domains. Additionally, we evaluate other domain invariance algorithms that do not rely on augmenta-

Table 2. Model accuracy of leave-one-domain-out evaluation on PACS. The best and second-best results are bold and underlined, respectively.

Methods	Art	Cartoon	Photo	Sketch	Avg.
DeepAll	84.94	76.98	97.64	76.75	84.08
FACT [35]	89.68		97.02		
SAM [33]	85.25	82.02	96.75	85.04 85.54	87.27
Ours	<u>88.98</u>	82.50	96.86	85.54	88.47

tion, including DANN [6, 18], DeepCORAL [26, 27], and ERM [21], LP-FT [16]. More details on the implementation settings are listed in Appendix.

4.2. Comparison Results

Figure 4 summarizes the in-domain (ID) and out-of-domain (OOD) performance for all methods across four real-world datasets: iWildCam, Camelyon17, BirdCalls, and Galaxy10. Each point represents one method, colors and shapes represent method types, and our method is marked as a red star.

Results on Real-World Datasets. Our method consistently achieves the best OOD performance across all four real-world datasets, while maintaining a strong ID performance. Notably, our approach significantly outperforms all generic methods, including generic augmentation and domain invariance baselines that do not require datasetspecific design or prior knowledge. Compared to the best generic method (FACT) on iWildCam, our method improves OOD Macro F1 from 34.7% to 36.8%. On Camelyon17, our approach achieves 96.4% OOD accuracy, outperforming the best generic augmentation (SAM at 92.2%) and the best domain invariance method (LP-FT at 91.4%). On BirdCall, OOD Macro F1 increases from 35.1% (FACT) to 40.7%, and on Galaxy10, our method improves OOD accuracy from 74.1% (SAM) to 83.4%. Overall, our method provides a more effective and generalizable way to improving OOD robustness.

Moreover, our method also outperforms **dataset-specific augmentation** methods Connect Later + Copy-Paste on iWildCam, Connect Later + Stain Color Jitter on Camelyon17, and Connect Later + Copy-Paste + Jitter on BirdCalls, all of which require expert knowledge and manual design tailored for the dataset based on its characteristics. In contrast, our method is in a fully **dataset-agnostic** way, but still achieves superior or comparable results. These results show that our method is not only effective but also broadly applicable, without relying on dataset-specific analysis or prior knowledge.

Table 3. Model accuracy of leave-one-domain-out evaluation on Digits-DG. The best and second-best results are bolded and underlined, respectively.

Methods	MNIST	MNIST-M	SVHN	SYN	Avg.
DeepAll	95.8	58.8	61.7	78.6	73.7
FACT [35]	97.9	65.6	72.4	90.3	81.5
SAM [33]	<u>97.8</u>	<u>66.8</u>	<u>73.2</u>	90.7	<u>82.1</u>
Ours	<u>97.8</u>	67.2	76.5	92.9	83.6

Table 4. Model accuracy of leave-one-domain-out evaluation on *OfficeHome*. The best and second-best results are bolded and underlined, respectively.

Methods	Art	Clipart	Product	Real	Avg.
DeepAll	57.88	52.72	73.50	74.80	64.72
FACT [35]	60.34	54.85	<u>74.48</u>	<u>76.55</u>	66.56
SAM [33]	60.79	<u>55.47</u>	74.37	76.37	<u>66.75</u>
Ours	64.69	55.65	<i>77.</i> 97	81.80	70.03

Results on Common Benchmarks. Tables 2, 3 and 4 summarize the leave-one-domain-out results on PACS, Digits-DG, and Office-Home. The results of FACT and SAM in these tables are copied from the source paper [33] for fair comparison, as our re-implementations under identical settings produced slightly lower numbers. In these tables, DeepAll refers to vanilla backbones trained from a simple aggregation of all source data [34]. Our method achieves the highest average accuracy on all three benchmarks (PACS: 88.47, Digits-DG: 83.6, Office-Home: 70.03). These results show that the proposed dual-space targeted augmentation is dataset-agnostic and robust to different domain variations, while our focus remains on real-world deployment/environment shifts.

5. Ablation Study

Table 5 presents ablation results of the effects of pixel-space and frequency-space mixing, as well as the impact of the gradient-guided mechanism. Across the four real-world datasets, our full method achieves the highest OOD performance, outperforming LP-FT [16] and all single-modality or an unguided variant (replacing the mixing map with unified mixing ratio in frequency space, denoted Ours_v1). Frequency-only mixing consistently outperforms pixel-only mixing—especially on Camelyon17 and Galaxy10—highlighting the importance of frequency-space perturbation. Replacing the gradient-guided mechanism (w/o grad-guide) leads to a consistent drop in OOD performance, confirming that this adaptive, sensitivity-aware guidance is essential for robust domain adaptation.

Table 5. Ablation results comparing LP-FT (Ours without augmentations), pixel-only, frequency-only, ours with unified interpolation ratio in frequency domain (Ours_v1), and our full method across four datasets.

	iWildCam (F1)		Camelyon17 (Acc)		BirdCall (F1)		Galaxy10 (Acc)	
	ID	OOD	ID	OOD	ID	OOD	ID	OOD
LP-FD	46.4	31.2	92.3	91.4	73.1	30.1	93.6	54.3
Pixel-only	45.4	29.1	87.5	69.8	75.2	32.4	95.5	68.2
Frequency-only	52.0	35.6	98.3	95.7	73.4	37.6	95.1	77.9
Ours_v1	51.3	36.3	98.7	<u>96.3</u>	75.7	38.3	95.7	80.8
Ours	<u>51.9</u>	36.8	<u>98.6</u>	96.4	<u>75.4</u>	40.7	<u>95.3</u>	83.4

Table 6. Comparison of connectivity across class, domain, and both for different methods on Camelyon17 and iWildCam datasets.

Dataset	Augmentations	α	β	γ	α/γ	β/γ
Camelyon17	w/o Augmentations	0.015	0.189	0.002	7.50	94.5
	RandAugment	0.181	0.186	0.114	1.59	1.63
	Stain Color Jitter	0.029	0.116	0.004	7.25	29.0
	Ours_v1	0.120	0.073	0.003	40.0	24.3
iWildCam	w/o Augmentations	0.007	0.008	0.021	0.33	0.38
	RandAugment	0.224	0.125	0.130	1.72	0.96
	Copy-Paste	0.254	0.031	0.063	4.03	0.49
	Ours_v1	0.212	0.030	0.051	4.16	0.59

5.1. Empirical Evaluations of Connectivity

To better understand why our method is effective on improving OOD robustness, we take iWildCam and Camelyon17 as examples and empirically evaluate the connectivity measures. The process of computing the average connectivity between two class-domain pairs (c, d) and (c', d')involves labeling all training examples from class c and domain d as 0, and those from class c' and domain d' as 1, while discarding examples from other classes or domains. Then, we train a ResNet50 [9] model (Training details are presented in Appendix). The test set is prepared similarly to the training set, and the model's performance on the test dataset provides an estimate of connectivity between the specified class-domain pairs, quantified by the test error rate. Specifically, we train binary classifiers from scratch to predict the class-domain pair of each input example. For iWildCam, we randomly select 15 class-domain pairs, while for Camelyon17, we use all class-domain pairs since it is a binary classification task. We use Ours_v1 for connectivity estimation to exclude the effect of gradient-adaptive modulation and focus on how dual-space mixing influences cross-domain feature connectivity.

We present connectivity ratios α/γ and β/γ on datasets Camelyon17 and iWIIdCam in Table 6. As shown in Table 6, our method achieves the highest α/γ value on both datasets, showing more consistent semantic alignment across domains as well as more effective randomization

of spurious domain-dependent features $x_{d:\text{spu}}$. However, a moderate β/γ indicates our method may also slightly perturbs class-relevant features $x_{\text{obj}}, x_{d:\text{robust}}$. However, from Table 5 and Figure 4, our method still achieves the best OOD performance. This result is consistent with the estimation proposed by Shen et al. [25], where the target accuracy is estimated to be $(\alpha/\gamma)^{w_1} \cdot (\beta/\gamma)^{w_2}$, with higher weight on α/γ (i.e., $w_1 > w_2$). These results show that our method achieves a balance of preservation of class-relevant features and perturbation of domain-relevant features.

6. Conclusion, Limitations and Future Work

We propose D-GAP, providing a simple and adaptive approach for OOD robustness without dataset-specific analysis. By operating in both frequency and pixel spaces and adaptively interpolating amplitude values, our method achieves notable improvements on multiple real-world datasets and common domain adaptation datasets.

One limitation is that the current framework needs additional gradient computation in every training batch during augmentation, which takes extra training time.

In future work, we aim to improve the efficiency of our gradient-adaptive augmentation mechanism. Moreover, integrating our augmentation scheme with foundation models or self-supervised objectives may further improve OOD robustness in label-scarce or zero-shot settings.

References

- [1] Peter Bandi, Oscar Geessink, Quirine Manson, Marcory Van Dijk, Maschenka Balkenhol, Meyke Hermsen, Babak Ehteshami Bejnordi, Byungjae Lee, Kyunghyun Paeng, Aoxiao Zhong, et al. From detection of individual metastases to classification of lymph node status at the patient level: the camelyon17 challenge. *IEEE transactions on medical imaging*, 38(2):550–560, 2018. 2
- [2] Sara Beery, Grant Van Horn, and Pietro Perona. Recognition in terra incognita. In *Proceedings of the European conference on computer vision (ECCV)*, pages 456–473, 2018. 1
- [3] Sara Beery, Arushi Agarwal, Elijah Cole, and Vighnesh Birodkar. The iwildcam 2021 competition dataset. *arXiv* preprint arXiv:2105.03494, 2021. 2
- [4] Ekin D Cubuk, Barret Zoph, Jonathon Shlens, and Quoc V Le. Randaugment: Practical automated data augmentation with a reduced search space. In *Proceedings of the IEEE/CVF conference on computer vision and pattern recognition workshops*, pages 702–703, 2020. 1, 6
- [5] Terrance DeVries and Graham W Taylor. Improved regularization of convolutional neural networks with cutout. *arXiv* preprint arXiv:1708.04552, 2017. 6
- [6] Yaroslav Ganin, Evgeniya Ustinova, Hana Ajakan, Pascal Germain, Hugo Larochelle, François Laviolette, Mario March, and Victor Lempitsky. Domain-adversarial training of neural networks. *Journal of machine learning research*, 17(59):1–35, 2016. 7
- [7] Irena Gao, Shiori Sagawa, Pang Wei Koh, Tatsunori Hashimoto, and Percy Liang. Out-of-domain robustness via targeted augmentations. In *International Conference on Machine Learning*, pages 10800–10834. PMLR, 2023. 1, 2, 3,
- [8] Ishaan Gulrajani and David Lopez-Paz. In search of lost domain generalization. In *International Conference on Learn*ing Representations, 2021. 1
- [9] Kaiming He, Xiangyu Zhang, Shaoqing Ren, and Jian Sun. Deep residual learning for image recognition. In *Proceedings of the IEEE conference on computer vision and pattern recognition*, pages 770–778, 2016. 8
- [10] Xilin He, Jingyu Hu, Qinliang Lin, Cheng Luo, Weicheng Xie, Siyang Song, Muhammad Haris Khan, and Linlin Shen. Towards combating frequency simplicity-biased learning for domain generalization. Advances in Neural Information Processing Systems, 37:31078–31102, 2024. 1
- [11] Dan Hendrycks, Steven Basart, Norman Mu, Saurav Kadavath, Frank Wang, Evan Dorundo, Rahul Desai, Tyler Zhu, Samyak Parajuli, Mike Guo, et al. The many faces of robustness: A critical analysis of out-of-distribution generalization. In *Proceedings of the IEEE/CVF international conference on computer vision*, pages 8340–8349, 2021. 1
- [12] Leung Henry. Galaxy10 decals dataset., 2021. 2
- [13] Maximilian Ilse, Jakub M Tomczak, and Patrick Forré. Selecting data augmentation for simulating interventions. In International conference on machine learning, pages 4555–4562. PMLR, 2021.
- [14] Alexis Joly, Hervé Goëau, Stefan Kahl, Lukáš Picek, Titouan Lorieul, Elijah Cole, Benjamin Deneu, Maximilien Serva-

- jean, Andrew Durso, Hervé Glotin, et al. Overview of lifeclef 2022: an evaluation of machine-learning based species identification and species distribution prediction. In *International Conference of the Cross-Language Evaluation Forum for European Languages*, pages 257–285. Springer, 2022. 2
- [15] Pang Wei Koh, Shiori Sagawa, Henrik Marklund, Sang Michael Xie, Marvin Zhang, Akshay Balsubramani, Weihua Hu, Michihiro Yasunaga, Richard Lanas Phillips, Irena Gao, et al. Wilds: A benchmark of in-thewild distribution shifts. In *International conference on* machine learning, pages 5637–5664. PMLR, 2021. 1, 2
- [16] Ananya Kumar, Aditi Raghunathan, Robbie Jones, Tengyu Ma, and Percy Liang. Fine-tuning can distort pretrained features and underperform out-of-distribution. In *International Conference on Learning Representations*, 2022. 5, 7
- [17] Da Li, Yongxin Yang, Yi-Zhe Song, and Timothy M Hospedales. Deeper, broader and artier domain generalization. In *Proceedings of the IEEE international conference on computer vision*, pages 5542–5550, 2017. 2, 3
- [18] Mingsheng Long, Zhangjie Cao, Jianmin Wang, and Michael I Jordan. Conditional adversarial domain adaptation. Advances in neural information processing systems, 31, 2018. 7
- [19] Daniel S Park, William Chan, Yu Zhang, Chung-Cheng Chiu, Barret Zoph, Ekin D Cubuk, and Quoc V Le. Specaugment: A simple data augmentation method for automatic speech recognition. arXiv preprint arXiv:1904.08779, 2019.
- [20] Hannah Pinson, Joeri Lenaerts, and Vincent Ginis. Linear cnns discover the statistical structure of the dataset using only the most dominant frequencies. In *International Con*ference on Machine Learning, pages 27876–27906. PMLR, 2023. 1
- [21] Helen Qu and Sang Michael Xie. Connect later: improving fine-tuning for robustness with targeted augmentations. In *Proceedings of the 41st International Conference on Machine Learning*, pages 41769–41786, 2024. 1, 3, 5, 6, 7
- [22] Shiori Sagawa, Pang Wei Koh, Tony Lee, Irena Gao, Sang Michael Xie, Kendrick Shen, Ananya Kumar, Weihua Hu, Michihiro Yasunaga, Henrik Marklund, et al. Extending the wilds benchmark for unsupervised adaptation. In *Inter*national Conference on Learning Representations, 2022. 2
- [23] Tim Sainburg and Asaf Zorea. Noisereduce: Domain general noise reduction for time series signals. arXiv preprint arXiv:2412.17851, 2024. 6
- [24] Ankita Sarkar, Sarbani Palit, and Ujjwal Bhattacharya. Demystifying galaxy classification: An elegant and powerful hybrid approach. In 2024 39th International Conference on Image and Vision Computing New Zealand (IVCNZ), pages 1–6. IEEE, 2024. 6
- [25] Kendrick Shen, Robbie M Jones, Ananya Kumar, Sang Michael Xie, Jeff Z HaoChen, Tengyu Ma, and Percy Liang. Connect, not collapse: Explaining contrastive learning for unsupervised domain adaptation. In *Interna*tional conference on machine learning, pages 19847–19878. PMLR, 2022. 3, 8
- [26] Baochen Sun and Kate Saenko. Deep coral: Correlation alignment for deep domain adaptation. In *Computer vision*—

- ECCV 2016 workshops: Amsterdam, the Netherlands, October 8-10 and 15-16, 2016, proceedings, part III 14, pages 443–450. Springer, 2016. 7
- [27] Baochen Sun, Jiashi Feng, and Kate Saenko. Correlation alignment for unsupervised domain adaptation. *Domain* adaptation in computer vision applications, pages 153–171, 2017. 7
- [28] David Tellez, Maschenka Balkenhol, Irene Otte-Höller, Rob Van De Loo, Rob Vogels, Peter Bult, Carla Wauters, Willem Vreuls, Suzanne Mol, Nico Karssemeijer, et al. Whole-slide mitosis detection in h&e breast histology using phh3 as a reference to train distilled stain-invariant convolutional networks. *IEEE transactions on medical imaging*, 37(9):2126– 2136, 2018. 3, 6
- [29] Hemanth Venkateswara, Jose Eusebio, Shayok Chakraborty, and Sethuraman Panchanathan. Deep hashing network for unsupervised domain adaptation. In *Proceedings of the IEEE conference on computer vision and pattern recogni*tion, pages 5018–5027, 2017. 2, 3
- [30] Guangze Wang. Galaxy morphology classification with densenet. In *Journal of Physics: Conference Series*, page 012064. IOP Publishing, 2023. 6
- [31] Shunxin Wang, Raymond Veldhuis, Christoph Brune, and Nicola Strisciuglio. What do neural networks learn in image classification? a frequency shortcut perspective. In *Proceedings of the IEEE/CVF International Conference on Computer Vision*, pages 1433–1442, 2023. 1
- [32] Olivia Wiles, Sven Gowal, Florian Stimberg, Sylvestre-Alvise Rebuffi, Ira Ktena, Krishnamurthy Dj Dvijotham, and Ali Taylan Cemgil. A fine-grained analysis on distribution shift. In *International Conference on Learning Representa*tions, 2021. 1
- [33] Chengchao Xu and Xinmei Tian. Semantic-aware mixup for domain generalization. In *2023 International Joint Conference on Neural Networks (IJCNN)*, pages 1–8. IEEE, 2023. 1, 4, 5, 6, 7
- [34] Qinwei Xu, Ruipeng Zhang, Ya Zhang, Yanfeng Wang, and Qi Tian. A fourier-based framework for domain generalization. In Proceedings of the IEEE/CVF conference on computer vision and pattern recognition, pages 14383–14392, 2021. 7
- [35] Qinwei Xu, Ruipeng Zhang, Ziqing Fan, Yanfeng Wang, Yi-Yan Wu, and Ya Zhang. Fourier-based augmentation with applications to domain generalization. *Pattern Recognition*, 139:109474, 2023. 1, 3, 4, 5, 6, 7
- [36] Shen Yan, Huan Song, Nanxiang Li, Lincan Zou, and Liu Ren. Improve unsupervised domain adaptation with mixup training. *arXiv preprint arXiv:2001.00677*, 2020. 1
- [37] Huaxiu Yao, Yu Wang, Sai Li, Linjun Zhang, Weixin Liang, James Zou, and Chelsea Finn. Improving out-of-distribution robustness via selective augmentation. In *International Conference on Machine Learning*, pages 25407–25437. PMLR, 2022. 1, 6
- [38] Sangdoo Yun, Dongyoon Han, Seong Joon Oh, Sanghyuk Chun, Junsuk Choe, and Youngjoon Yoo. Cutmix: Regularization strategy to train strong classifiers with localizable features. In *Proceedings of the IEEE/CVF international con*ference on computer vision, pages 6023–6032, 2019. 1, 6

- [39] Hongyi Zhang, Moustapha Cisse, Yann N Dauphin, and David Lopez-Paz. mixup: Beyond empirical risk minimization. arXiv preprint arXiv:1710.09412, 2017. 6
- [40] Kaiyang Zhou, Yongxin Yang, Timothy Hospedales, and Tao Xiang. Deep domain-adversarial image generation for domain generalisation. In *Proceedings of the AAAI conference* on artificial intelligence, pages 13025–13032, 2020. 1, 2, 3